2020 IEEE/RSJ International Conference on Intelligent Robots and Systems (IROS)
October 25-29, 2020, Las Vegas, NV, USA (Virtual)

The Multi-material Actuator for Variable Stiffness (MAVS): Design, Modeling, and Characterization of a Soft Actuator for Lateral Ankle Support

Carly M. Thalman†, *Student Member, IEEE*, Tiffany Hertzell†, Marielle Debeurre, and Hyunglae Lee*, *Member, IEEE*

***Abstract*— This paper presents the design of the Multi-material Actuator for Variable Stiffness (MAVS), which consists of an inflatable soft fabric actuator fixed between two layers of rigid retainer pieces. The MAVS is designed to be integrated with a soft robotic ankle-foot orthosis (SR-AFO) exosuit to aid in supporting the human ankle in the inversion/eversion directions. This design aims to assist individuals affected with chronic ankle instability (CAI) or other impairments to the ankle joint. The MAVS design is made from compliant fabric materials, layered and constrained by thin rigid retainers to prevent volume increase during actuation. The design was optimized to provide the greatest stiffness and least deflection for a beam positioned as a cantilever with a point load. Geometric programming of materials was used to maximize stiffness when inflated and minimize stiffness when passive. An analytic model of the MAVS was created to evaluate the effects in stiffness observed by varying the ratio in length between the rigid pieces and the soft actuator. A finite element analysis (FEA) was generated to analyze and predict the behavior of the MAVS prior to fabrication. The results from the analytic model and FEA study were compared to experimentally obtained results of the MAVS. The MAVS with the greatest stiffness was observed when the gap between the rigid retainers was smallest and the rigid retainer length was smallest. The MAVS design with the highest stiffness at 100 kPa was determined, which required 26.71 $\pm$ 0.06 N to deflect the actuator 20 mm, and a resulting stiffness of 1,335.5 N/m and 9.1% margin of error from the model predictions.**

Keywords - Soft Robot Applications, Soft Actuator Modeling, Soft Robot Materials and Design, Wearable Robots.

I. Introduction

Permanent deformation of the tendons surrounding the ankle joint can occur in individuals suffering from chronic ankle instability (CAI), which is a long-term disability that often arises as a result of recurrent ankle sprains [1], [2]. Lateral ankle buckling causes sudden instances of ankle inversion-eversion (IE) in the frontal plane, which creates excessive stress in the tendons and results in the ankle sprain [2]. An estimated 85% of reported ankle sprains are a result of such injuries, and repeated occurrences of sprained ankles can lead to CAI [3], [4]. An affected individual is at an increased risk of injury, trips, and falls with the onset of CAI, as the damaged tendons surrounding the ankle joint may lead to an irregular gait pattern [2], [5], [6]. Traditional rigid ankle-foot orthoses (AFOs), those most commonly prescribed to treat CAI, are made out of lightweight plastics that lend their stiffness to the ankle joint, thereby preventing lateral ankle buckling from a trip, fall, or other irregular ankle motion [5], [7], [8]. The stiff AFO brace lines the ankle's medial and lateral malleolus, which prevents such IE motions during walking [5], [7]–[11]. However, due to the rigidity of their materials, traditional AFOs can limit ankle motion and fix ankle angle in a specific orientation, which can further degrade an already impaired gait [12].

Fig. 1. Design of the SR-AFO exosuit with an anchoring strap on the knee (4) and a connecting strap (3) to the inflatable fabric-based actuator for plantar/dorsiflexion support (1). The SR-AFO is shown incorporating the Multi-material Actuator for Variable Stiffness (MAVS) in (2).

The field of wearable robotics seeks to address deficiencies in providing assistance to humans during certain motions or actions, or to improve on existing passive wearable devices and technologies [13]–[18]. However, some challenges of rigid exoskeletons tend to revolve around cost, weight, size, and require computing power [7], [19]. Such challenges have given rise to soft robotic solutions, which couple traditional robotic control theory with flexible, often cost-effective, materials. Wearable soft robots are typically more lightweight and comfortable for the user to wear, and provide a more forgiving interaction between the robot and the human as the compliant materials alleviate issues with joint alignment [16], [20]. These benefits have motivated previous studies for ankle rehabilitation, where a soft wearable robot for the ankle can effectively conform to support and correct irregular gait patterns with simplified control algorithms and actuation methods. Soft robotic applications have been rising in popularity in recent years, as demonstrated in [21], [22], but applications to address CAI and lateral ankle sprain are limited.

In previous work [23], a soft robotic AFO (SR-AFO) counterpart to traditional rigid AFOs was proposed to assist in IE ankle support and gait rehabilitation with the use of pneumatic fabric actuators. This work expands upon the previous SR-AFO design further reduce actuation time and increase ankle stiffness. This paper presents the Multi-material Actuator for Variable Stiffness

* Corresponding Author
† Equally Contributing First Authors
Carly M. Thalman, Tiffany Hertzell, Marielle Debeurre, and Hyunglae Lee are with the Ira A. Fulton Schools of Engineering, Arizona State University, AZ , USA. cmthalma@asu.edu, thertzel@asu.edu, mdebeurr@asu.edu, hyunglae.lee@asu.edu

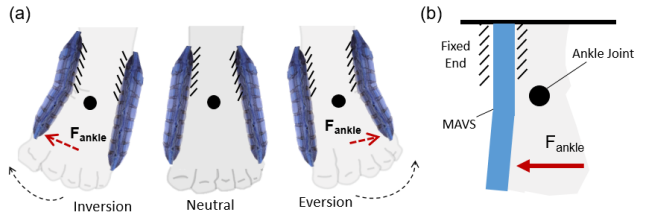

Fig. 2. (a) Placement of the MAVS on the ankle joint in the neutral position, the inversion position, and the eversion position to help resist and prevent medial and lateral buckling. (b) shows the basic principles behind the creation of the modeling of the MAVS and cantilever beam orientation against the ankle.

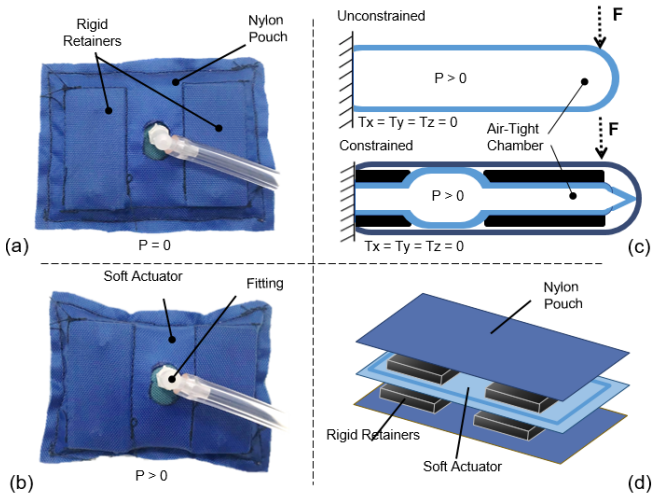

Fig. 3. (a) The MAVS shape when deflated and (b) when inflated with the main components of the actuator specified. (c) A simplified representation of the MAVS with and without the rigid retainers fixed in a cantilever beam setup with a point load applied. (d) An exploded view of the MAVS displaying the different layers.

(MAVS). The MAVS is designed to be integrated into the SR-AFO exosuit as shown in Fig. 1. The SR-AFO design [24] uses pneumatic solenoid valves to control actuation. The MAVS is pneumatically actuated using soft fabric actuators, which will be used to increase IE ankle stiffness when actuated by being placed along the medial and lateral sides of the ankle joint. The targeted use-case for the MAVS is for gait rehabilitation, and therefore actuator latency and slow inflation times can cause issues in exosuit performance [25], [26].

To reduce actuator latency, the volume of the actuator is minimized to decrease the time needed for the actuator to reach a fixed pressure with a set airflow from the valves. The increased IE ankle stiffness prevents ankle buckling while walking and will correct gait irregularities with SR-AFO use. Further descriptions of the MAVS design, testing methods, and results are presented in Sections II-IV. Section II outlines the design, modeling, and fabrication of the MAVS. Section III presents the characterization and experimental evaluation of the MAVS actuator designs, and describes the experimental results. Section IV discusses in detail the overall MAVS performance, design strengths and considerations, and future plans for modifications and development.

II. Design and Modeling

A. Modeling

1) Analytic Model: One inspiration for the new actuator design comes from the sliding layer laminate concept by Jiang and Gravish [27]. The concept in the aforementioned paper focuses on a three layer laminate that has different levels of stiffness based on the

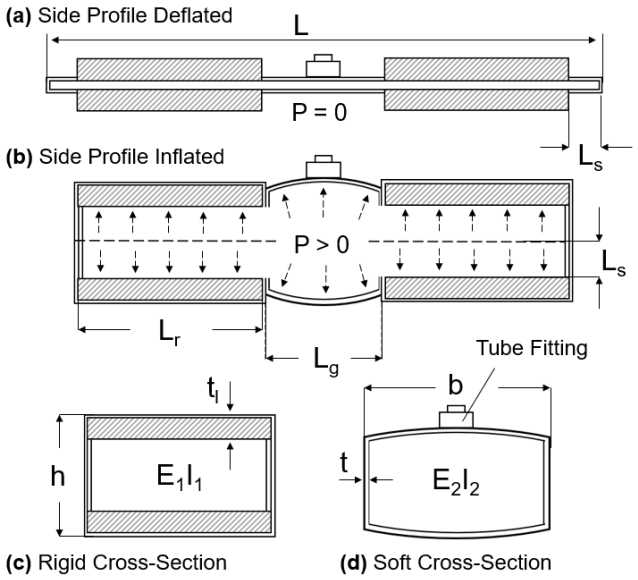

Fig. 4. (a) The side profile of the MAVS when passive and (b) when the MAVS is inflated. (c) The cross-section view of the rigid retainer section and (d) the cross-section view of the exposed soft actuator section.

orientation of the rigid layers. The stiffest orientation of the laminate layers with the smallest deflection was found to be when the rigid pieces are aligned together. The design created for the MAVS integrates this idea by having an inflatable actuator secured between two layers of rigid pieces embedded in fabric. The rigid pieces are aligned on the top and bottom of the actuator. By integrating the small rigid pieces into a compliant fabric actuator, the pieces in the outer layers act as retainers that reduce the total volume of the actuator when inflated. This design constrains the actuator so that it will be flush with the user while inflated. Incorporating small rigid pieces helps achieve greater stiffness while not inhibiting user comfort or gait. A single segment of the MAVS weights only between 31.2 g - 89.3 g, depending on the configuration used. A similar design to the MAVS for the SR-AFO incorporates rigid pieces onto an inflatable actuator designed for contraction [28].

The design for the MAVS includes the similar concept that having a rigid piece secured to an inflatable actuator will restrict the total volume. Limiting the boundaries of the MAVS during inflation and restricting the vertical expansion resulted in higher stiffness at smaller volumes. The reduced volume allows for faster actuation time. Based on the model of a simply supported cantilever beam with a single point load at the free end and using Timoshenko's theory, the deflection of an inflatable beam can be modeled [29]–[31]. This modeling method uses the following equation for calculating deflection,

$$V(x) = \frac{F}{(E+P/S_o)I_o}\left(\frac{{l_o}^2 x}{2} - \frac{x^3}{6}\right) + \frac{Fx}{(P+kGS_o)} \tag{1}$$

where $V(x)$ is the deflection of an actuator of length l_o, which can be calculated at a length x away from the fixed end $x = 0$. The beam is subject to an internal pressure P and a transverse force F at the free end, where $x = l_o$. P is the global load due to the pressure applied at the ends of the beam. The shear coefficient is represented by kGS_o, where k is determined by the cross-sectional shape and Cowper's formulation [32], S_o is the cross-sectional area, and G is the shear modulus of the material. The shear modulus is calculated for the Polylactic Acid (PLA) filament used to 3D print the rigid retainers and Nylon fabric with the equation,

$$G = \frac{E}{2(1+\nu)} \tag{2}$$

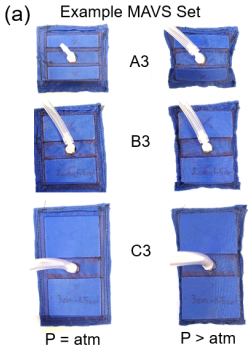

(b)

L_g (cm)	L_r (cm) 1	2	3
0.5	A1	B1	C1
1	A2	B2	C2
1.5	A3	B3	C3
2	A4	B4	C4
2.5	A5	B5	C5
3	A6	B6	C6

Fig. 5. (a) A visual of the different iterations of the MAVS when deflated and inflated, (b) the different gap and rigid retainer lengths used in the different iterations represented by a letter and number label.

where ν is Poisson's ratio and E is the Elastic Modulus, which is determined by the material properties. The second moment of inertia, I_o, is determined by the shape of the cross-sectional area and the axis about which the actuator is being deflected. From Cowper's formulation of a thin-walled box section, k can be calculated with,

$$k = \frac{10(1+\nu)(1+3m)^2}{(12+72m+150m^2+90m^3)} + \ldots \tag{3}$$

$$\frac{10(1+\nu)(1+3m)^2}{\nu(11+66m+135m^2+90m^3)+10n^2((3+\nu)m+3m^2)}$$

where

$$m = \frac{bt_l}{ht} \tag{4}$$

and

$$n = \frac{b}{h} \tag{5}$$

The maximum deflection can be calculated using $x = l$, [29], which reduces Eq. (1) to,

$$V(l) = -\frac{F}{2Pbh}l - \frac{Fl^3}{3Ebh^2} \tag{6}$$

where b is the base length of the cross-sectional area, which is kept constant at 4 cm for each iteration, h is the height of the actuator when inflated, and l is the length of the actuator. The total length l of the actuator is calculated as

$$l = 2L_s + N(L_r + L_g) + L_r \tag{7}$$

where l is the total length of the MAVS, L_s is the length added by the seam, L_r is the length of the rigid piece, and L_g is the length of the gap between rigid pieces where the soft actuator is exposed. The number of exposed sections of the soft actuator is represented by N to account for varying lengths. This is later used to calculate the total length of the MAVS when it is extended to be applied to supporting the ankle. The total deflection $V_t(x)$ of the MAVS is then calculated by,

$$V_t(x) = N(V_{PLA} + V_{Nylon}) + V_{PLA} \tag{8}$$

for an actuator with N segments of different materials. The variables V_{PLA} and V_{Nylon} indicate the deflections calculated from Eq. (6) using the material properties of PLA and Nylon.

Two main parameters were varied and evaluated using this model: (1) the length of the rigid retainer and (2) the size of the gap exposing the soft actuator. For the first parameter, three values were chosen mainly for fabrication and practicality restrictions. The three different widths chosen were 1 cm, 2 cm, and 3 cm, labeled L_r in Fig. 4. The three rigid retainer widths were labeled A, B, and C, respectively, and the gap widths were labeled 1 - 6, respectively,

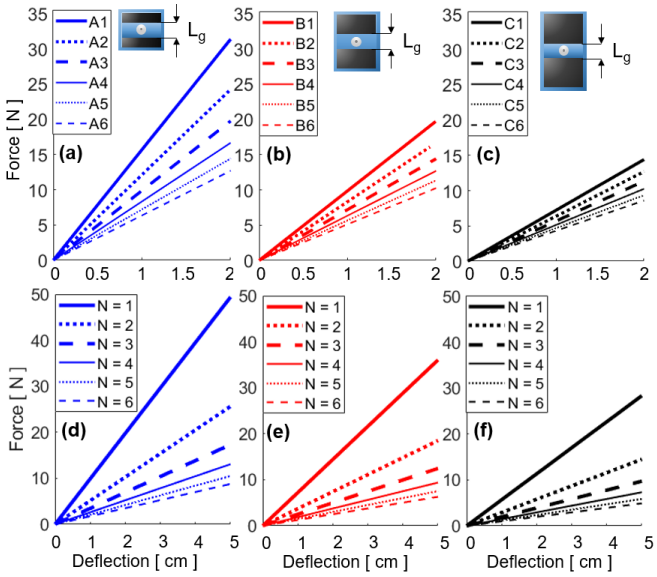

Fig. 6. Graphs (a)-(c) show the stiffness outputs of the MAVS for varying rigid retainer size (A, B, and C) with varying gap sizes (1-6), graphs (d)-(f) show the stiffness for various values of N, which is how many sections of soft actuator are exposed for actuator design $A3$.

as denoted in Fig. 5. Lengths of the rigid retainers below 1 cm were determined to be too small to easily implement in fabrication, and a length of longer that 3 cm was determined as too large and bulky for the end application of placing the actuator on the ankle for support. The second parameter, L_g, was varied from 0.5 cm to 3 cm in increments of 0.5 cm. It was limited to 0.5 cm in the lower bound for fabrication purposes, as the tube fitting could not be inserted into a smaller gap. The upper bound of the parameter was also set to 3 cm, as going beyond this gap size would increase the volume beyond what is desired for fast inflation. The complete list of these parameters and the corresponding labeling system can be seen in Fig. 5. These conditions were evaluated using Eq. (8) to determine which set of parameters and dimensions would be ideal for the MAVS. Internal actuator pressure was held constant at the maximum operating pressure used by the SR-AFO (100 kPa) and each condition from Fig. 5 was evaluated. A linear relationship between beam deflection and the resultant force was observed and can be seen in Fig. 6. MAVS designs with smaller rigid retainers (L_r) showed increased resistance to the transverse loads than actuators with the same net gap size and larger rigid retainers. Increasing the gap size (L_g) indicates a decrease in stiffness for a fixed retainer size.

The MAVS were evaluated for varying lengths by incrementally increasing N, which in turn increased the number of sections where the soft actuator is exposed and not constrained by the rigid retainers. The benefit to a larger surface area of the soft actuator relates to the behavior of the entire MAVS when deflated, which would inherently become more compliant than actuators that were designed to have a higher surface area composed of the rigid retainers. The drawback to increasing N is that less of the soft actuator is constrained and allowed to expand. This increases the overall volume of the actuator and as a result, the inflation time will inherently increase with N. The model was adjusted to evaluate the performance of the actuator with values of N increasing from 1 - 6 for each of the three rigid retainer lengths (A,B, and C) and a fixed L_g of 1.5 cm. Based on the model predictions, the higher stiffness values occur at the smaller values of L_g, and decrease as more actuator is exposed. Therefore, the smallest 3 values of L_g will be evaluated more thoroughly to determine which iteration of the MAVS would be best suited for the SR-AFO exosuit, and has the highest stiffness when pressurized, and the lowest stiffness when

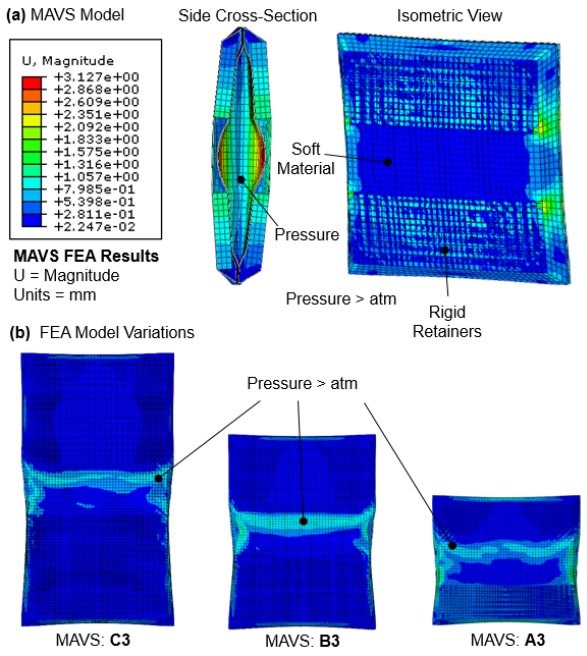

Fig. 7. A visual representation of the models used to simulate the MAVS using finite element analysis (FEA). (a) Shows an unconstrained MAVS model in both a cross-sectional view from the side, and an isometric view of the MAVS. These two viewports help provide clear visualization of the internal layers and behaviors of the iterations between materials. (b) shows the MAVS actuator in 3 orientations: the $C3$ - $A3$ configuration models are shown at $P > 0$ to demonstrate how the model reflects the fabricated models.

passive.

2) Finite Element Modeling: In order to observe the behavior of each MAVS prior to fabrication, a finite element analysis (FEA) software was used to predict the accuracy of the analytic model and to validate the behavior of the stacked materials. The FEA simulation was run using Abaqus CAE (ABAQUS, Dassault Systems, Vlizy-Villacoublay, France) in a dynamic explicit environment. The major benefit of being able to model the MAVS is to show the interaction between multiple layers of several material types, thicknesses, and properties. This allows the internal chambers of the MAVS to be observed and studied as done in other works with variable stiffness actuators [33].

Two thin 2D homogeneous shells were used to create each layer of the fabric actuator and stacked vertically, and sectioned partitions of the shell faces were tied to create the heat-sealed seams. The rigid pieces were modeled using solid 3D homogeneous extrusions. The TPU coated nylon was simulated using a Young's Modulus of 498.9 *MPa*, a Poisson's ratio of 0.35, and a material thickness of 0.15 *mm*. The PLA rigid pieces were modeled using material properties with a Young's Modulus of 3600 *MPa* and a Poisson's ratio of 0.3 as used in previous works [34]. The two thin shells were placed in an assembly and stacked vertically and sealed to create a seam around the perimeter. The rigid pieces were placed on the top and bottom faces of the actuator at a pre-defined gap distance as shown in Fig. 8. Finally, another thin 2D homogeneous shell was placed to encase the soft actuator and rigid pieces. The outward faces of the rigid pieces were tied to the outer shell and a global interaction property for surface-surface contact was applied to the assembly. A solid 3D homogeneous clamp was created from the PLA material property and fixed at $T_x = T_y = T_z = 0$ to hold the actuator at a fixed point for the cantilever beam example modeled in the previous section.

Two loads were applied to the model: (1) a uniform pressure load to the internal faces of the thin shells of the actuator, and (2) a transverse load applied at a fixed point at the end of the actuator beam. A total of three steps were run for the simulation: (1)

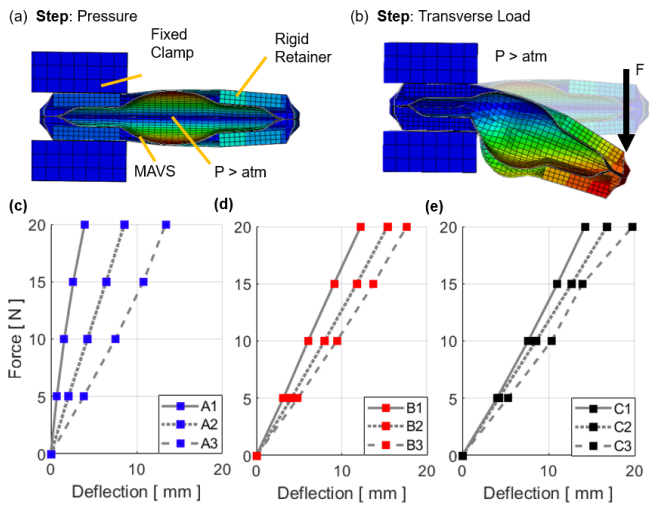

Fig. 8. A finite element analysis (FEA) is used to model the behavior of the materials ad layers within the MAVS. The FEA simulation is run with the MAVS (a) placed in a cantilever orientation and inflated, and (b) subjected to a transverses point load while deflection is measured. This is done for 5 N, 10 N, 15 N, and 20 N for MAVS sets $A-C$ for each of these conditions (c - e).

Pressurization, (2) Stabilization, (3) Point Load as depicted in Fig. 8(a - c). The deflection of the MAVS was measured by fixing one half of the MAVS along the y-axis, and applying a perpendicular force to the free end. Deflection was measured as the change in the angle from the starting position of the inflated actuator to the final position of the free end of the MAVS as shown in Fig. 8. A transverse load of 5 N, 10 N, 15 N, and 20 N was applied at a fixed point on the free end of the actuator, which was inflated to 100 *kPa*. This was done for the three highest performing MAVS from sets $A-C$ predicted by the analytic model in Fig. 5(a - c). The deflection of the end of the actuator was measured along the same axis as the transverse load for MAVS sets $A1-A3$, $B1-B3$, and $C1-C3$. The results in Fig. 8 indicated the same behavior in the MAVS stiffness as the parameters of L_g and L_r were varied. As L_g increased, the stiffness of the MAVS decreased. This behavior was also seen in L_r, with decreasing resistance to deflection as the rigid retainer increased in length.

B. Fabrication

The first of the three layer design is composed of rigid Polylactic Acid (PLA) 3D Printer Filament (1.75 diameter *mm* PLA 3D Printer Filament, HATCHBOX) sewn between two layers of fabric. Two layers of the embedded rigid retainers were used to encase an inflatable actuator in between. The soft actuator fabricated uses thermoplastic polyurethane (TPU) coated nylon fabric (200 Denier Rockywoods Fabrics) which is thermally bonded with a 2 *mm* heat impulse sealer (AIE-500 2 *mm* Impulse Sealer, American International Electric INC, CA) which applies uniform heat and pressure to the seam to create an air-tight seal [34]. A sewing machine is used to create stitching to hold the rigid retainers in place, as well as to hold the layers together. The MAVS consists of a total of three main layers as shown in Fig. 9 from left to right: 1x fabric-based inflatable actuator, and 2x layers of nylon material with the rigid retainers embedded into the layers. The inflatable chamber was sealed at the designated location to create a rectangular shape using the impulse sealer on three of the four sides. The fourth side was left open for the installation of the pneumatic fitting. A small hole was cut into the fabric and the threaded nylon barbed nozzle and nut fitting were secured onto the TPU coated nylon. The final side was sealed with the impulse sealer to create an air-tight seal that is the same net shape as the entire actuator. The additional two layers were fabricated using the same method for each.

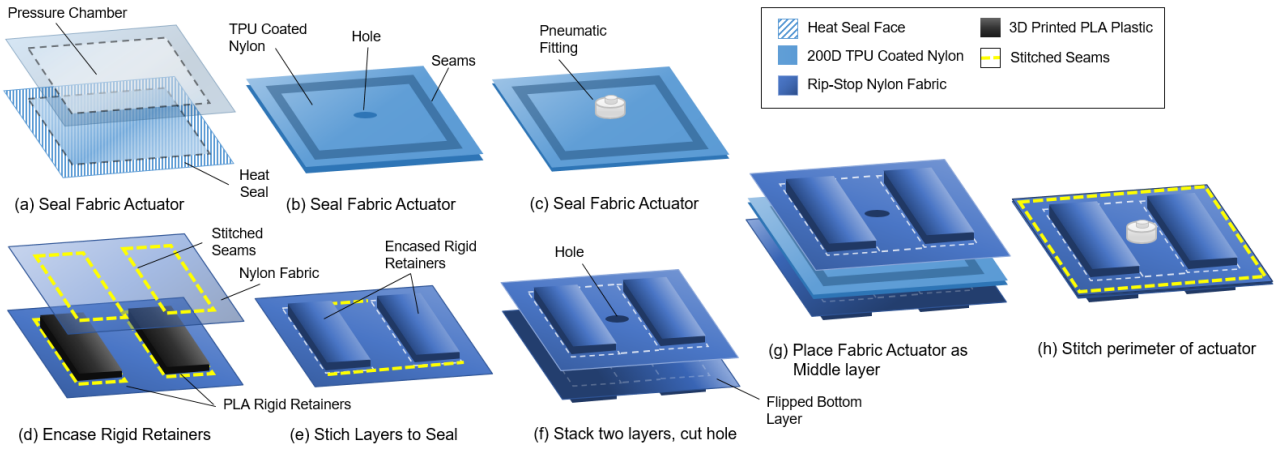

Fig. 9. The fabrication process for the MAVS shown in steps where (a) shows the TPU coated nylon with marked boundaries for heat sealing, (b) shows the fabric once it is sealed and has a hole made for step (c) where a pneumatic fitting is secured. Step (d) shows the three layers that make-up the rigid retainer layer, step (e) shows the rigid retainers tightly sewn into the Nylon, and step (f) shows the two outer layers that will secure the inflatable actuator. (g) Shows the fabricated layers stacked in order and (h) shows where the layers are secured together.

The rigid retainers were 3D printed using PLA and have a thickness of 2 *mm* and a width of 40 *mm*, while the length was varied for each iteration of the MAVS parameterization, as well as the placement distance between the rigid retainers. Each of the constraining layers was made from two pieces of nylon fabric, which were stacked with the rigid retainers placed in between at fixed distances for designs *A*, *B*, or *C*. A sewing machine (SE-400 Brother, Bridgewater, NJ) was used to create a stitched seam around the net shape of the rigid retainers, encasing the parts between the two nylon layers. This was done to create the top and bottom constraining layers. A hole was cut into the top constraining layer to allow the tube fitting from the soft actuator to fit in between the rigid retainers. The sealed soft actuator was placed in between the two constraining layers as shown on the right side of Fig. 9, with the fitting centered within the hole cut previously into the top constraining layer. A final seam was sewn in a rectangular shape around the rigid retainers, at a 5 *mm* offset. This seam allowance provided a buffer to avoid sewing into the sealed soft actuator, and to provide an offset that constrains vertical expansion during inflation. In order to determine the performance of the proposed design, a variety of MAVS were fabricated in order to evaluate a range of parameters and compare to the analytic and FEA results.

III. Actuator Characterization

A. Experimental Setup

A universal tensile testing machine (UTM) (Instron 5565, Instron Corp., High Wycombe, United Kingdom) was used to measure the stiffness and deflection of the MAVS designs. Each iteration was tested at varying pressures from 0 *kPa* to 100 *kPa* in increments of 10 *kPa*. A custom clamp was fabricated to fix the MAVS in place while being subjected to deflection testing. The MAVS had a tab sewn into the free end to interface with the clamps paired with the load cell of UTM as seen in Fig. 10(b). This allowed for the UTM to apply a point load to the MAVS while it is fixed in a cantilever position. The UTM pulled the free end of the MAVS upward 20 *mm*. The tab acted as a constant point of contact so that the lever arm distance did not change. In the case of applying a load downward on the MAVS, the point of contact changed because the probe would slide across the top of the MAVS as it pushed down on it, thus changing the length of the lever arm. To keep the most consistent point load location, the tabs were used to deflect the MAVS upward. Each iteration was deflected upward and the force in Newtons was taken so that the stiffness of each MAVS could be determined.

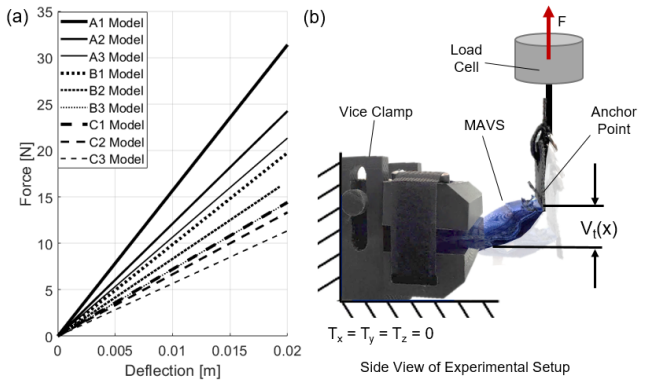

Fig. 10. The average force for each MAVS when deflected from 0 to 20 *mm* is shown for the predicted highest performing sets that were tested (a). The test setup for each of the sets is shown (b), with a MAVS fixed in the custom clamp while being subjected to a vertical, transverse load from the UTM.

B. Results

1) Passive Actuator Stiffness: Since the MAVS is being designed to be integrated into wearable exosuits, the ideal MAVS would have minimal to negligible stiffness while passive. This criterion is to prevent the passive MAVS from impacting the user's range of motion or comfort level when the device is not providing active assistance. The MAVS were evaluated as a passive cantilever beam using the UTM. The MAVS were clamped in place and the load cell moved to the fixed displacement of 20 *mm*, which is the highest displacement the smallest *A*1 MAVS can achieve, and results in final deflection angles sufficient to cover the motion of IE of the ankle. The resulting force was measured across three separate trials for each of the 18 MAVS design iterations. Fig. 11 shows the resulting force required to deflect the passive MAVS. It can been observed that *A*1 and *A*2 have the highest stiffness when passive. This is due to the smallest ratios of exposed soft actuator to the rigid retainers. MAVS *A*3 produced a slight stiffness increase, however the force to the 20 *mm* displacement reached only just above 1 *N* and is still significantly low. All other MAVS fell below 1 *N*, which is considered negligible for the considered application.

2) Active Actuator Stiffness: The MAVS was evaluated using the custom vice clamp and UTM for the most optimal conditions predicted by the analytic model. The model predicted that the smaller L_g values used, the higher the resulting stiffness. This was validated through experimentally obtained results on the UTM.

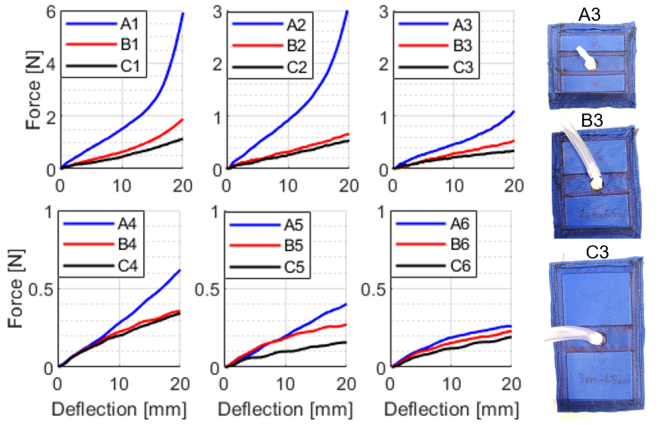

Fig. 11. The passive MAVS stiffness comparing each rigid retainer length (A, B, and C) for each gap length (1-6) compared against each together to determine least stiff design.

MAVS designs for $A1-3$, $B1-3$, and $C1-3$ where $N=1$ were evaluated on the bench, with one end of the MAVS fixed in the vice clamp and the other end was free to move vertically. For these trials, the MAVS was held constant at 100 kPa to allow for comparison of varied geometries.

The trends of each MAVS followed closely to the model predictions for each evaluated condition. MAVS $A1$ required the highest force to reach a 20 mm deflection, reaching 32.59 $\pm$ 1.43 N with a calculated stiffness of 1,629.4 N/m, which fell within 4.5% of the model predictions (Fig. 12(a)). MAVS $A2$ was the second highest stiffness values observed at 100 kPa, reaching 26.71 $\pm$ 0.06 N with a calculated stiffness of 1,335.5 N/m and fell within 9.1% of the model predictions. The third highest stiffness MAVS was MAVS $A3$, which obtained 22.74 $\pm$ 0.2 N, with a calculated stiffness of 1,137.0 N/m, and fell within 11.1% of the predicted value. This trend continues in order from MAVS $B1$, $B2$, and $B3$, with the maximum force output observed at 19.36 $\pm$ 0.45 N, 16.09 $\pm$ 0.22 N, and 14.74 $\pm$ 0.35 N, respectively (Fig. 12(b)). The decrease in the force required to achieve the fixed deflection was also observed with the last section of MAVS, where $C1$ = 16.71 $\pm$ 0.50 N, $C2$ = 16.49 $\pm$ 0.39 N, and 14.20 $\pm$ 0.05 N (Fig. 12(c)). The values obtained for the $C1-C3$ MAVS showed very similar results to that of the $B1-B3$ MAVS set, though had a much greater volume due to the overall larger net shape. The $B1-B3$ MAVS set had a similar force requirement to deflect 20 mm and a smaller net shape, which reduced volume. However, the $A1-A3$ set had a far higher stiffness with the smallest volume of all options.

3) Actuator Stiffness at Varied Pressures: The MAVS were also evaluated across various pressure levels, where the maximum force required to achieve 20 mm of deflection was recorded at each pressure interval. The pressure was varied between 10 kPa and 100 kPa, in increments of 10 kPa. Fig. 12 (d)-(f) shows the maximum force of each MAVS evaluated across each pressure level. Force required for deflection had a linear relationship to increasing pressure. The same relations were observed for the geometries of the MAVS design, where the A set resulted with the highest force requirement, the B set was in the middle range, and the C set showed the lowest resistance to bending.

IV. Discussion

This paper presents the design, modeling and characterization of a new soft actuator design with varying stiffness, designed for application in lateral ankle support in the existing SR-AFO exosuit (though is not limited to use only with this application). The MAVS uses fabric-based inflatable actuators constrained by thin rigid retainer pieces that limit the vertical expansion of the fabric layers to physically restrict the volume of the internal pressure

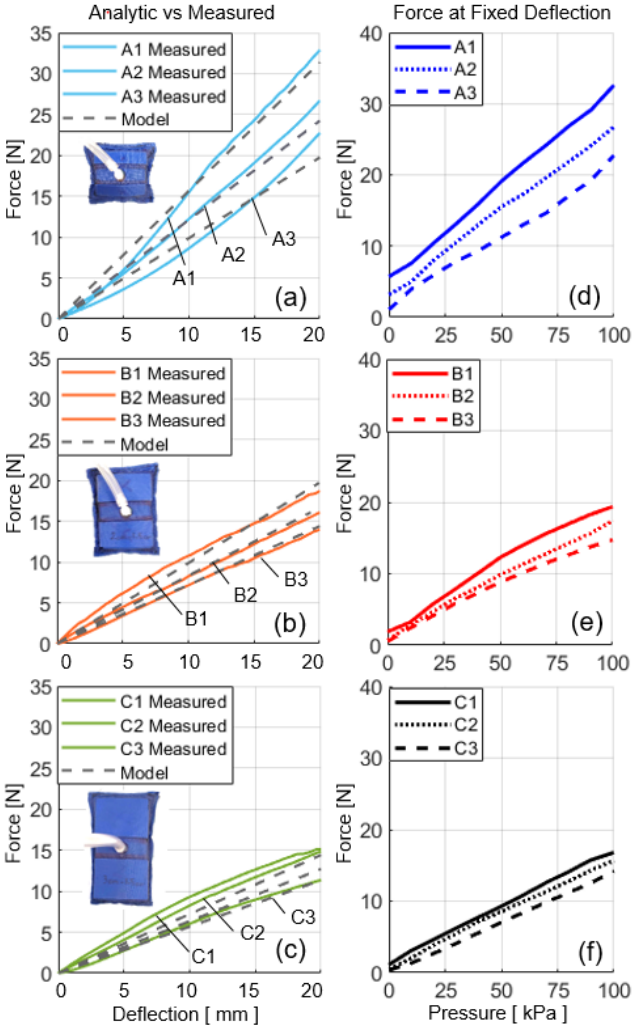

Fig. 12. (a)-(c) Show the measured values for $A1-A3$, $B1-B3$, and $C1-C3$ with the analytic model plotted for reference. (d)-(f) Shows the force curve as the pressure is increased for a deflection of 20 mm for each iteration with designs A, B, and C graphed separately.

chamber. A model was created to evaluate ideal geometries of various parameters on the MAVS, primarily the lengths of the rigid pieces compared to the length of the exposed soft actuator. A finite element analysis was used to evaluate how the rigid pieces interact as predicted with the multiple layers. The model was run for the geometries predicted to produce the highest stiffness. Since the model predicted that most MAVS in the C category would have relatively low stiffness when pressurized, as well as actuators with larger values of L_g, it can be assumed that the MAVS in these lower categories can be omitted for higher stiffness when pressurized. The passive MAVS stiffness test omitted MAVS $A1$ due to high passive stiffness. MAVS $A2$ saw an increase, but the resulting stiffness was observed at half that of $A1$, and therefore $A2$ was still considered a viable solution.

The MAVS were evaluated experimentally using a UTM that displaced the free end of the MAVS when fixed as a cantilever beam. The force was recorded using a load cell on the UTM, and the displacement was tracked. A fixed displacement was used to serve as a baseline for the comparison between all trials, and the pressure was fixed at 100 kPa. The top three MAVS geometries were selected from each size range of the rigid pieces to determine the relationship between the gap of exposed soft actuator and restricted sections of the soft actuator from the rigid retainers. The experimental results showed that the most effective MAVS were

the $A2$ and $A3$ MAVS, which had the highest stiffness values when active, and lower stiffness values when passive. MAVS $A2$ required and observed force of 26.71 ± 0.06 N at 100 kPa and fell within 9.1% of the model predictions. MAVS $A3$, which obtained 22.74 ± 0.2 N and falling within 11.1% of the predicted value, which had a larger error than $A2$. Therefore, the final MAVS design determined to be the best suited for the SR-AFO is the $A2$ MAVS, with a rigid retainer of $L_r = 1$ cm and a gap of exposed soft actuator at $Lg = 1$ cm.

Future work will begin to evaluate the MAVS embedded into the SR-AFO with varying lengths using the model prediction of length based on Fig. 6, where increasing N values were anticipated. This factor is anticipated to have a high dependence on the individual wearing the SR-AFO, as individuals with longer or shorter ankle length may require larger or smaller actuator lengths. Additionally, the MAVS will be evaluated with dynamic walking trials using a dual-axis robotic platform as used in previous studies in quiet standing [23], [35]. The response time and recoil effects of the actuator will also be evaluated.

ACKNOWLEDGEMENTS

C. M. Thalman is funded by the National Science Foundation, Graduate Research Fellowship Program (NSF-GRFP) award #1841051. This work is funded by the Global Sport Institute of the adidas and Arizona State University (ASU) Global Sport Alliance.

REFERENCES

[1] J. G. Garrick. The frequency of injury, mechanism of injury, and epidemiology of ankle sprains. *The American journal of sports medicine*, 5(6):241–242, 1977.

[2] K. Venesky, C. L Docherty, J. Dapena, and J. Schrader. Prophylactic ankle braces and knee varus-valgus and internal-external rotation torque. *Journal of athletic training*, 41(3):239, 2006.

[3] D. J. Caine, C. G. Caine, and K. J. Lindner. Epidemiology of sports injuries. *The Nurse Practitioner*, 21(9):142, 1996.

[4] MS Yeung, Kai-Ming Chan, CH So, and WY Yuan. An epidemiological survey on ankle sprain. *British journal of sports medicine*, 28(2):112–116, 1994.

[5] J F Geboers, M R Drost, F Spaans, H Kuipers, and H A Seelen. Immediate and long-term effects of ankle-foot orthosis on muscle activity during walking: a randomized study of patients with unilateral foot drop. *Archives of physical medicine and rehabilitation*, 83(2):240–245, 2002.

[6] J. F Lehmann, S. M Condon, B. J de Lateur, and J C Smith. Ankle-foot orthoses: effect on gait abnormalities in tibial nerve paralysis. *Archives of physical medicine and rehabilitation*, 66(4):212–218, 1985.

[7] P Malcolm, S Lee, S Crea, C Siviy, F Saucedo, I Galiana, F A Panizzolo, K G Holt, and C J Walsh. Varying negative work assistance at the ankle with a soft exosuit during loaded walking. *Journal of neuroengineering and rehabilitation*, 14(1):62, 2017.

[8] I. Wiszomirska, M. Błażkiewicz, K. Kaczmarczyk, G. Brzuszkiewicz-Kuźmicka, and A Wit. Effect of drop foot on spatiotemporal, kinematic, and kinetic parameters during gait. *Applied bionics and biomechanics*, 2017, 2017.

[9] R B Stein, D G Everaert, A K Thompson, S Chong, M Whittaker, J Robertson, and G Kuether. Long-term therapeutic and orthotic effects of a foot drop stimulator on walking performance in progressive and nonprogressive neurological disorders. *Neurorehabilitation and neural repair*, 24(2):152–167, 2010.

[10] P. M Kluding, K. Dunning, M. W O'dell, S. S Wu, J. Ginosian, J. Feld, and K. McBride. Foot drop stimulation versus ankle foot orthosis after stroke: 30-week outcomes. *Stroke*, 44(6):1660–1669, 2013.

[11] J. S Jaivin, J. O Bishop, W G Braly, and H S Tullos. Management of acquired adult dropfoot. *Foot & ankle*, 13(2):98–104, 1992.

[12] M J Mueller, S D Minor, J A Schaaf, M J Strube, and S A Sahrmann. Relationship of plantar-flexor peak torque and dorsiflexion range of motion to kinetic variables during walking. *Physical therapy*, 75(8):684–693, 1995.

[13] B Shi, X Chen, Z Yue, S Yin, Q Weng, X Zhang, J Wang, and W Wen. Wearable ankle robots in post-stroke rehabilitation of gait: A systematic review. *Frontiers in neurorobotics*, 13:63, 2019.

[14] J. Kwon, J. Park, S. Ku, Y. Jeong, N. Paik, and Y.L. Park. A Soft Wearable Robotic Ankle-Foot-Orthosis for Post-Stroke Patients. *IEEE RA-L, International Conference on Soft Robotics (RoboSoft)*, 2019.

[15] J. Chung, R. Heimgartner, C. T. O'Neill, N. S. Phipps, and C. J. Walsh. Exoboot, a soft inflatable robotic boot to assist ankle during walking: Design, characterization and preliminary tests. In *2018 7th IEEE International Conference on Biomedical Robotics and Biomechatronics (Biorob)*, pages 509–516. IEEE, 2018.

[16] Y.L. Park, B.R. Chen, N.O. Pérez-Arancibia, D. Young, L. Stirling, R.J. Wood, E.C. Goldfield, and R. Nagpal. Design and control of a bio-inspired soft wearable robotic device for ankle-foot rehabilitation. *Bioinspiration & biomimetics*, 9(1):016007, 2014.

[17] S. Lee, S. Crea, P. Malcolm, I. Galiana, A. Asbeck, and C. Walsh. Controlling negative and positive power at the ankle with a soft exosuit. In *IEEE International Conference on Robotics and Automation (ICRA)*, pages 3509–3515. IEEE, 2016.

[18] Y. Ren, Y. Wu, C. Yang, T. Xu, R. L. Harvey, and L. Zhang. Developing a Wearable Ankle Rehabilitation Robotic Device for in-Bed Acute Stroke Rehabilitation. *IEEE Transactions on Neural Systems and Rehabilitation Engineering*, 2017.

[19] R. Browning, J. R. Modica, R. Kram, and A. Goswami. The effects of adding mass to the legs on the energetics and biomechanics of walking. *Medicine & Science in Sports & Exercise*, 39(3):515–525, 2007.

[20] A.T. Asbeck, R.J. Dyer, A.F. Larusson, and C.J. Walsh. Biologically-inspired soft exosuit. In *2013 IEEE 13th International Conference on Rehabilitation Robotics (ICORR)*, pages 1–8, 2013.

[21] G. Bao, H. Fang, L. Chen, Y. Wan, F. Xu, Q. Yang, and L. Zhang. Soft robotics: Academic insights and perspectives through bibliometric analysis. *Soft Robotics*, 5(3):229–241, 2018.

[22] M. Cianchetti, C. Laschi, A. Menciassi, and P. Dario. Biomedical applications of soft robotics. *Nature Reviews Materials*, 3(6):143–153, 2018.

[23] C. M. Thalman and H Lee. Design and validation of a soft robotic ankle-foot orthosis (sr-afo) exosuit for inversion and eversion ankle support. In *2019 International Conference on Robotics and Automation (ICRA)*. IEEE, 2020.

[24] C. M. Thalman, T Hertzell, and H Lee. Toward a soft robotic ankle-foot orthosis (sr-afo) exosuit for human locomotion: Preliminary results in late stance plantarflexion assistance. In *IEEE International Conference on Soft Robotics, (RoboSoft)*. IEEE, 2020.

[25] P Malcolm, W Derave, S Galle, and D De Clercq. A simple exoskeleton that assists plantarflexion can reduce the metabolic cost of human walking. *PloS one*, 8(2), 2013.

[26] Y. Ding, M. T. Tolley, Y. Park, Robert F. Shepherd, Robert J. Wood, Michael Wehner, Yiğit Mengüç, Annan Mozeika, Cagdas Onal, and George M. Whitesides. Pneumatic Energy Sources for Autonomous and Wearable Soft Robotics. *Soft Robotics*, 2014.

[27] M. Jiang and N. Gravish. Sliding-layer laminates: a robotic material enabling robust and adaptable undulatory locomotion. In *2018 IEEE/RSJ International Conference on Intelligent Robots and Systems (IROS)*, pages 5944–5951. IEEE, 2018.

[28] J. Kwon, S. Yoon, and Y. Park. Flat inflatable artificial muscles with large stroke and adjustable force–length relations. *IEEE Transactions on Robotics*, 2020.

[29] C. Wielgosz and J-C Thomas. Deflections of inflatable fabric panels at high pressure. *Thin-walled structures*, 40(6):523–536, 2002.

[30] J. Thomas and Anh LE VANa. Inflatable beams subjected to axial forces. 2019.

[31] C Wielgosz, JC Thomas, and A Le Van. Mechanics of inflatable fabric beams. In *International Conference on Computational & Experimental Engineering and Sciences Honolulu, Hawaii, USA*, 2008.

[32] GR Cowper. The shear coefficient in timoshenko's beam theory. 1966.

[33] T Sun, Y Chen, T Han, C Jiao, B Lian, and Y Song. A soft gripper with variable stiffness inspired by pangolin scales, toothed pneumatic actuator and autonomous controller. *Robotics and Computer-Integrated Manufacturing*, 61:101848, 2020.

[34] C. M. Thalman, J. Hsu, L. Snyder, and P. Polygerinos. Design of a soft ankle-foot orthosis exosuit for foot drop assistance. In *2019 International Conference on Robotics and Automation (ICRA)*, pages 8436–8442. IEEE, 2019.

[35] V. Nalam and H. Lee. Design and validation of a multi-axis robotic platform for the characterization of ankle neuromechanics. In *2017 IEEE International Conference on Robotics and Automation (ICRA)*, pages 511–516. IEEE, 2017.